

Sensitivity and vibration reduction of buffeting induced resonance of hangers

Zhitian Zhang^{*1,2} and Weifeng Zhang^{1a}

¹Wind Engineering Research Center, Hunan University, Changsha, 410082, China

²Hunan Provincial Key Laboratory for Wind Engineering and Bridge Engineering, Changsha, 410082, China

(Received July 19, 2016, Revised June 8, 2017, Accepted June 9, 2017)

Abstract. Buffeting induced resonance (BIR) of hangers on long-suspension bridges is briefly reviewed, including mechanism and experimental verification. Taken the Xihoumen suspension bridge as a numerical example, sensitivities of the BIR of hangers to wind properties are investigated, including types of wind spectrum, turbulence intensity, and spacial coherence of wind fluctuations. Numerical simulations indicate that the BIR of hangers occur to both cases of different wind spectra, showing that it is insensitive to types of wind spectrum. On the other hand, it is found that the turbulence intensity affects buffeting of main cables almost in a linear manner, and so it does to the BIR of the hangers; however, the resonance factors, namely the ratio of the response of the hanger to that of the main cable, are little affected by the turbulence intensity. The spacial coherence of the wind fluctuations, although plays an important role on the buffeting responses of the main structure, has no substantial effects on the BIR of the hangers. Finally, replacement of steel strand with CFRP material has been verified as a very effective countermeasure against the BIR of hangers.

Keywords: bridge; hanger; buffeting; resonance; wind property; countermeasure

1. Introduction

Due to a number of mechanisms, flexible stay-cables and hangers at long-span cable-supported bridges are susceptible to sorts of wind-induced oscillations. Common types among them are rain-wind induced oscillations (Hikami and Shiraishi 1988, Matsumoto *et al.* 2003), wake-induced oscillations (Cigada *et al.* 1997 etc.), and wind-induced oscillations of dry cables (Miyata *et al.* 1994, Cheng *et al.* 2003, Macdonald *et al.* 2006, Matsumoto *et al.* 2010, Raeesi *et al.* 2013, Zuo *et al.* 2010, etc.). Recently, based on field observations (see Fig. 1) and numerical simulation, Zhang and Ge (2015) reported a new mechanism of wind-induced oscillations of hangers on suspension bridges; that is, buffeting of the main cables induced resonance of hangers.

According to field observations of the Xihoumen suspension bridge in China, large amplitude oscillations of hangers occurred on only several long hangers adjacent to the bridge towers (images are shown in Fig. 1). Major properties of the observed kind of oscillation include: (i) Violent oscillations occurred on hangers at both the side span and the center span, and the most

*Corresponding author, Professor, E-mail: zhangzhitian@hnu.edu.cn

^a Ph.D. Student, Email: b1201s012@hnu.edu.cn

violent ones locate in zones adjacent to the bridge towers. (ii) For the hangers oscillating most violently, the four separated ropes of each hanger were oscillating in an almost, but not fully synchronized manner. (iii) The mean wind direction oriented largely perpendicular to the bridge axis, and hangers were oscillating in a lateral direction, perpendicular to the bridge deck axis. (iv) Dominant frequency of the vibration is about 0.4Hz.

This kind of oscillation happened in both rainy and sunny days. By reasoning, Zhang *et al.* (2015) excluded the mechanisms of vortex-induced oscillations, galloping or wake galloping, and rain-wind induced oscillations. It was observed in wind tunnel that wake-induced galloping did occur due to aerodynamic interference among the 4 separated steel ropes of a single hanger (see Fig. 2). It was found, however, that the oscillations were sensitive to the wind directions, and the occurrence was limited to a narrow range of wind directions and to the ropes located in the wake of others. This is not in accordance with several field observations different in wind speeds and directions, and not in accordance with the phenomenon that all ropes experienced oscillation, regardless of leeward or windward. Therefore, wake galloping cannot be taken as a justified explanation. To date, two kinds of countermeasures have been tried successively on the hangers by the bridge administration department. Referring to Fig. 2, the first tried one was viscoelastic dampers, and they were reportedly invalid to the oscillations. Later, separators were installed on the hangers.

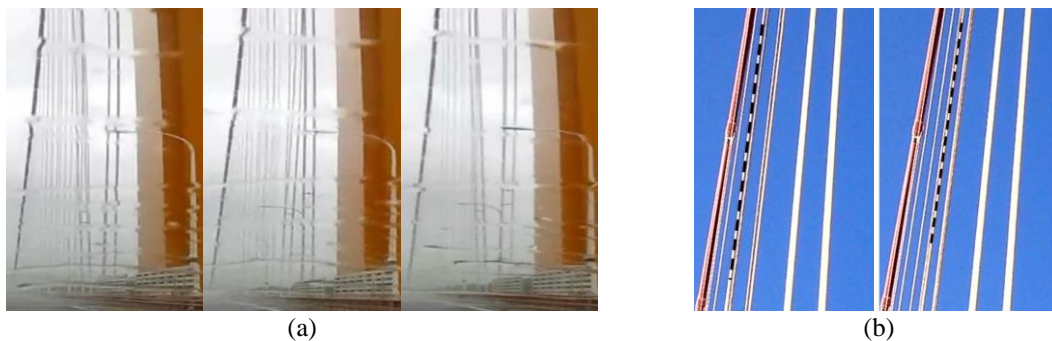


Fig. 1 Images of hanger oscillations: (a) in rainy day and (b) in sunny day

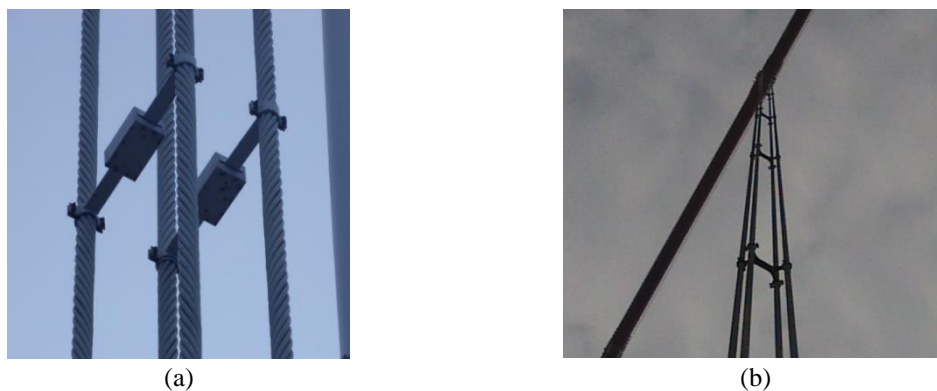


Fig. 2 Countermeasures for vibration reduction of the hangers at the Xihoumen bridge: (a) original dampers and (b) newly installed separators

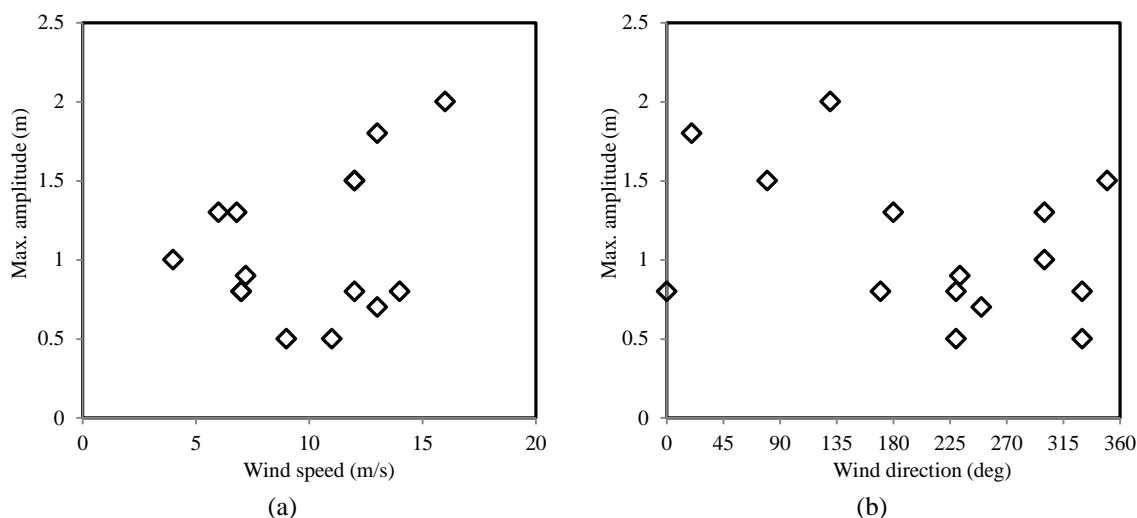


Fig. 3 Hanger oscillations at the Great belt east bridge (Data from Laursen *et al.* 2006): (a) Max. amplitudes versus wind speeds and (b) Max. amplitudes versus wind directions

What observed recently after the installation of separators is, however, four ropes linked with separators oscillating as a whole under moderate wind speeds, with large amplitudes.

Similar oscillations also occurred on the Great Belt east bridge (Laursen *et al.* 2006). As at the Xihoumen suspension bridge, severe oscillations at the Great Belt east bridge were also limited to several long hangers, and the data presented by Laursen *et al.* (2006) indicated no direct connections among the maximum oscillations, the mean wind speeds, and the wind directions (see Fig. 3). These known facts verify collectively that what observed on this bridge should also be characterized as buffeting induced resonance (BIR), since buffeting is determined by structural and turbulence properties, and is not connected directly to the mean wind speeds and directions in a simple manner.

In this study, the sensitivity of BIR of hangers to wind field properties is addressed, as well as a promising countermeasure against this kind of oscillation. Since detailed properties of the wind field were not able to be recorded, it is favorable to investigate the sensitivity of BIR to some turbulence properties via numerical simulations.

2. Qualitative analysis

2.1 Exclusion of wake galloping

A number of causes could result in cable vibrating. It was observed in the case of Xihoumen bridge, however, that not all hangers were in objectionable vibration, and violent oscillations were limited to the long hangers. Wake galloping is due to existence of a mean shear wind field, where the oscillator obtains energy from the wind flow over one complete oscillating period.

A basic property of wake galloping can exclude it from a possible explanation of the observed oscillation. Referring to Fig. 4, given the stiffness matrix of the leeward conductor as

$$[E] = \begin{bmatrix} E_{xx} & E_{xz} \\ E_{xz} & E_{zz} \end{bmatrix} \quad (1)$$

the critical condition of wake galloping is then determined by the following inequality (Price 1975)

$$\varepsilon^2 [(C_{\bar{L}x} - C_{\bar{D}z})^2 - (C_{\bar{D}x} - C_{\bar{L}z})^2] + (1 - k^2) [\varepsilon (C_{\bar{D}x} - C_{\bar{L}z})(C_{\bar{L}x} + C_{\bar{D}z}) - (1 - k^2) C_{\bar{L}x} C_{\bar{D}z}] \geq 0 \quad (2)$$

where

$$k^2 = \frac{E_{zz}}{E_{xx}}, \quad \varepsilon = \frac{E_{xz}}{E_{xx}} \quad (3)$$

$$C_{\bar{D}x}, C_{\bar{D}z}, C_{\bar{L}x}, C_{\bar{L}z} = a \frac{\partial C_D}{\partial x}, a \frac{\partial C_D}{\partial z}, a \frac{\partial C_L}{\partial x}, a \frac{\partial C_L}{\partial z} \quad (4)$$

where a is a constant for a specific pair of conductors and is independent on the length of the conductors. C_D, C_L are the aerodynamic drag and lift coefficients of the leeward conductor. x and z are relative horizontal and vertical distances between conductor centers expressed in diameters

$$x = \bar{x}/d, \quad z = \bar{z}/d \quad (5)$$

where d is the diameter of the conductor. For the hangers installed at the bridge concerned, $k^2 \approx 1$ and $\varepsilon \approx 1$. Hence the inequality (4) reduces to

$$(C_{\bar{L}x} - C_{\bar{D}z})^2 - (C_{\bar{D}x} - C_{\bar{L}z})^2 \geq 0 \quad (6)$$

It can be seen that the critical condition is virtually determined by the quasi-steady aerodynamic properties of the leeward steel wire ropes, and it is independent on the structural dynamic properties of hangers, which differ among hangers of different length. However, observations from the site indicate that only several long hangers near the bridge tower experienced severe oscillations. In view of this, wake galloping can be excluded.

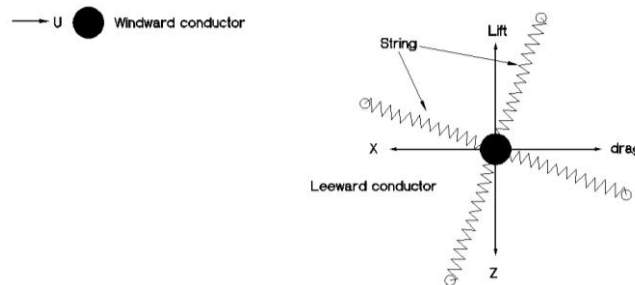


Fig. 4 Model for wake galloping of a leeward conductor

2.2 Exclusion of vortex-induced oscillation

Unsteady load fluctuations due to vortex shedding develop on a steel wire rope when it is put in a wind. Both upstream and downstream ropes contribute to this part of fluctuations. Depending on the Reynolds number, the range of Strouhal number of a circular is

$$St = fd/U = 0.2 \sim 0.4 \quad (7)$$

where f is the frequency of the shedding of vortex from the circular.

Regardless of whether the vortex shedding is harmonic or stochastic, the dominant frequency should not be far away from the range determined by Eq. (7). Hence, according to the wind velocity and the rope diameter, one has

$$f = St \times U/d \approx 50 \sim 100\text{Hz} \quad (8)$$

Obviously this frequency range is far away from the observed frequency, 0.4 Hz; hence, the observed phenomenon can be anything but vortex-induced vibration.

2.3 Exclusion of wind-rain induced oscillation

Although it was raining when the typhoon ‘Haikui’ hit this bridge, fundamental preconditions necessitate wind-rain induced oscillations are absent. For one thing, the hangers are not inclined but vertically installed, and the surface of the steel wire ropes is spiral and quite coarse. Hence a rivulet, which is essential for wind-rain induced oscillation, has no chance to be formed. Moreover, later after typhoon ‘Haikui’ hit the bridge, oscillation of hangers have been observed during sunny days (see Fig. 1(b)). Therefore, the possibility wind-rain excitation can be excluded.

2.4 Wake of the bridge tower

Naturally one may ask whether it is the tower’s wake that leads to the hangers’ vibration, since most severe oscillations occurred in the vicinity of the bridge tower. First, it can be seen from Fig. 5 that the hangers are actually located quite far away from the wake region, especially when the wind flow comes perpendicular to the bridge axis. Second, no matter what the wind direction was, it is impossible for all the four regions shown in Fig. 5 to be affected. What observed indicated that, however, hangers at all these regions experienced severe oscillations. Hence, the aerodynamic influence from the towers’ wake should not be a right explanation.

2.5 Buffeting induced resonance (BIR)

According to the video, there was almost no vehicle on the bridge when typhoon ‘Haikui’ hit it. Hence, vehicle induced vibration can be excluded either. Finally, one thing for certain is the oscillation must come from the action of the wind flow. Natural wind and wind-induced loads are stochastic, and hence structures immersed in wind response stochastically. Moreover, both the wind- and load-fluctuations are of broad-spectrum characteristics. Consequently, a bridge structure as a whole experiences broad-spectrum buffeting responses, and the main cables can be the most evident in this regard due to their abundance in natural modes. All hangers are attached to the main cables at their upper ends. Therefore, the main cables in vibration can be a source of excitation to

the hangers. Since natural frequencies of the hangers vary gradually with their lengths, there is a possibility of resonance for those hangers whose natural frequencies match with the main cable frequencies, especially with those relating to modes of high vibrating energy.

If BIR is the cause of the observed cable oscillation, then it could occur in various situations that differ in wind speeds, wind directions, and turbulence properties, as observed in site. In this sense, to reproduce BIR, it is unnecessary to know or to simulate the specific wind properties corresponding to an observed BIR.

3. Experimental verification of BIR

A simplified experimental set-up in wind tunnel is designed to verify this kind of oscillation. As shown in Fig. 6, a main cable is simulated by a rigid circular steel tube, of which one end is translationally fixed and the other end is elastically supported in the z -direction, allowing for lateral oscillation only. The natural frequency of the circular tube can be adjusted by changing the tension in the steel cord A. The hanger is simulated by a copper wire distributed with short aluminum cylinders. The vertically mounted hanger is attached to the steel tube on the upper end, and its lower end passes through a tiny hole in a fixed steel plate and then is attached immediately to a suspending weight. The target frequency of the hanger can be obtained by adjusting the attached suspending weight. Accelerometers are installed respectively on the steel tube and the hanger to record their responses. Further, to compare responses with and without the wind loads developed directly on the hanger itself, an organic glass shield was designed to enclose the whole hanger from the top to bottom (see Fig. 7). Details regarding the set-up are listed in the work of Zhang *et al.* (2015).

The frequency of the steel tube is modelled to target one of the natural frequencies of the main cables, which is the one closest to the observed resonance frequency, according to modal analysis using the FE model of the prototype bridge. It was found that significant internal resonance happened between the steel tube and the hanger attached to it (see Fig. 8), disregarding whether or not the hanger is enclosed in the glass shield. The steel tube absorbs energy from turbulence, exhibiting in stochastic vibrations which result in intermittent resonance of the attached hanger.

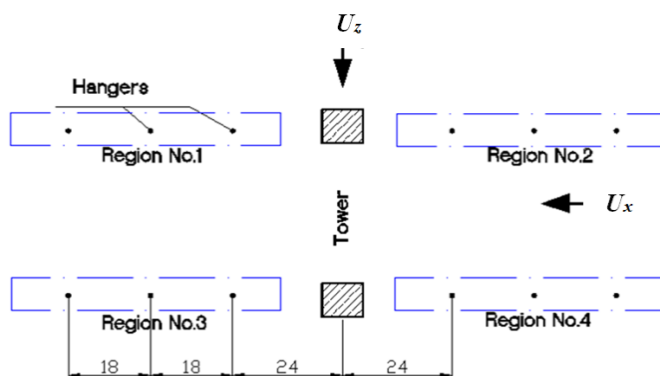


Fig. 5 Zones of severe oscillation near the bridge tower (unit:m)

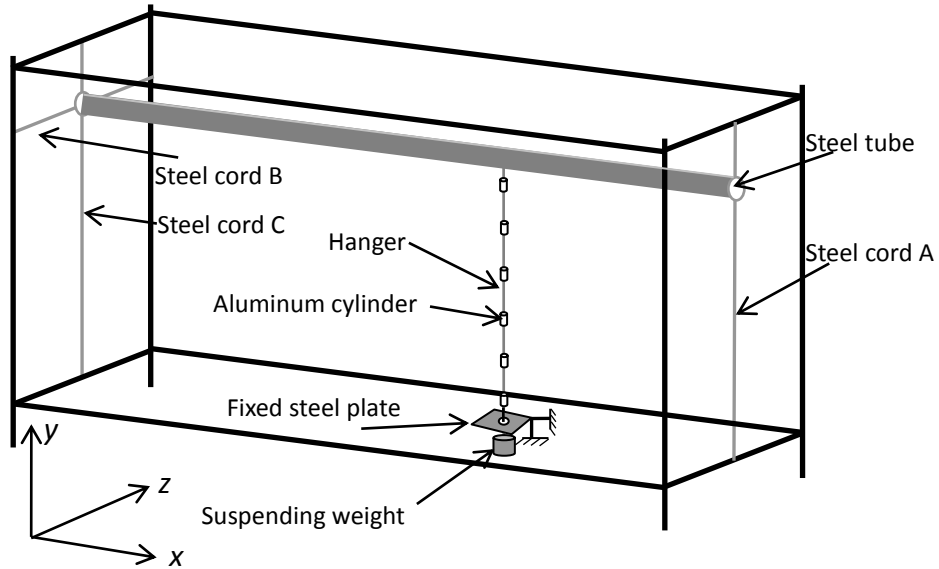


Fig. 6 Sketch of the experimental set-up

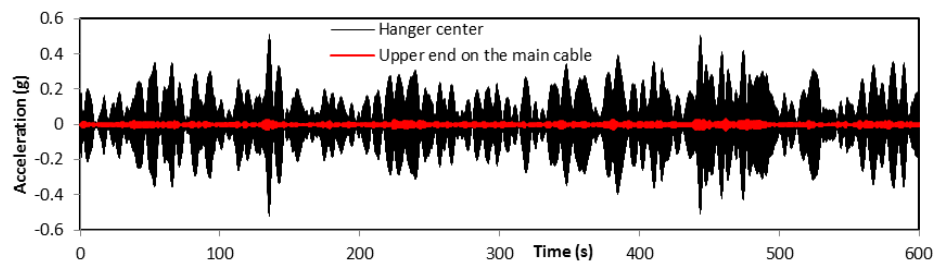


(a)



(b)

Fig. 7 Photos of experimental set up: (a) without glass shield and (b) with glass shield



(a)

Continued-

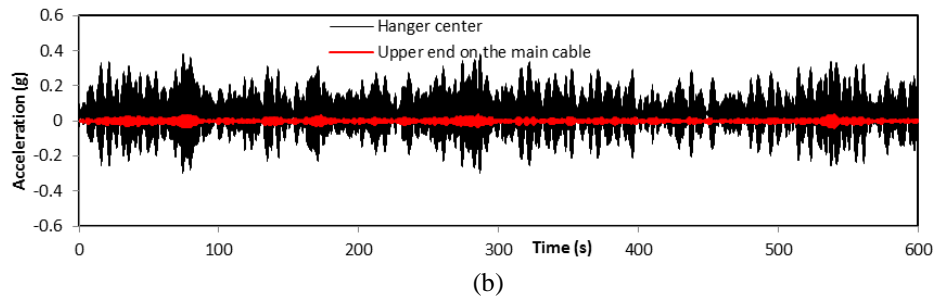


Fig. 8 Acceleration of the hanger center, $U = 4.71$ m/s: (a) Hanger enclosed in glass shield and (b) Hanger exposed in wind

4. Sensitivity to turbulence properties

4.1 FE model

The bridge concerned is a part of the project connecting the ZhouShan islands with the mainland China. It is now the second longest suspension bridge in the world with a main span of 1650 m, a twin-box girder with a slot of 6.0 m in width. Fig. 9 shows the panoramic view of the bridge, of which the FE model has 957 nodes and 1197 elements in total. 3-D bar element (3 DOF for each node) is used for all hangers and cables, while 3-D beam elements (6 DOF for each node, shear strain not included) are used for bridge deck and towers.

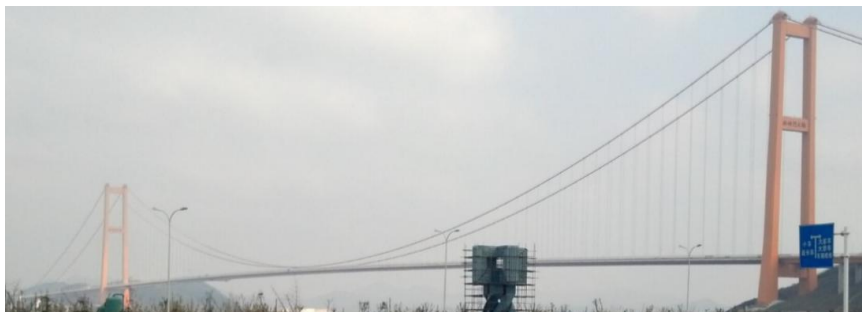


Fig. 9 Panoramic view of the Xihoumen suspension bridge

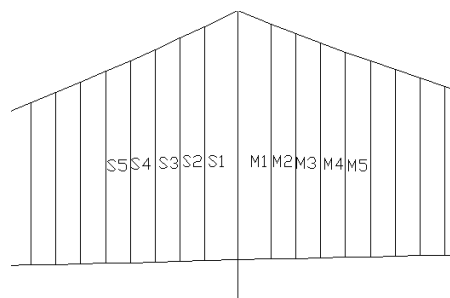


Fig. 10 Layout of hangers with refined meshes

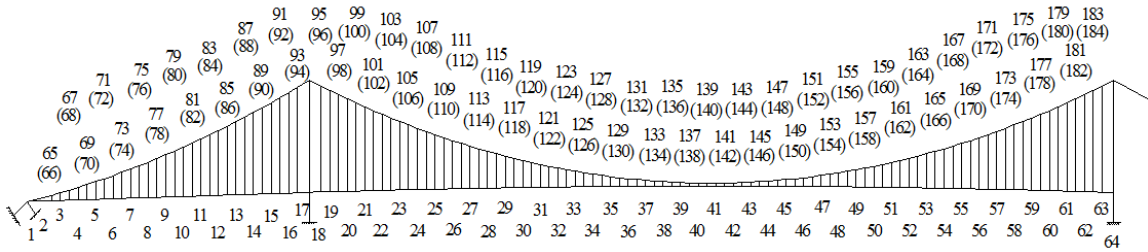


Fig. 11 FE model and wind field discretization

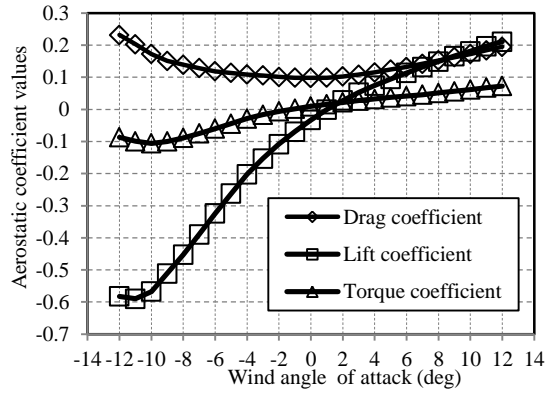


Fig. 12 Aerostatic load coefficients

Initial strain in the bar elements have been taken into account to avoid stiffness matrix singularity. Since oscillations of the long hangers are what concerned, a refined meshing is set to the 10 longest hangers adjacent immediately to the north tower (5 on the side span, S1 to S5, and 5 on the main span, M1 to M5, see Fig. 10); each hanger is divided into 11 elements, sufficient to simulate modal responses of low-to-medium frequencies.

The wind field simulated is divided into 184 discr

ete points (see Fig. 11). Aerostatic forces exerting on the bridge deck include drag, lift, and pitching moment while those on the main cables include drag only. Aerostatic coefficients of the bridge deck tested with a sectional rigid model are plotted in Fig. 12. Wind loads are updated every time step (with a step length of 0.1s) according to turbulent wind components.

4.2 Wind field simulation and wind loads

Turbulent wind fields used in this work are simulated with the spectral representation method developed by Deodatis (1996). The simulated mean wind profile is plotted in Fig. 13, and the description of it is given as

$$U(z) = \frac{u_*}{k} \ln \frac{z - z_d}{z_0} \quad (9)$$

where u_* denotes the shear velocity of the oncoming flow; k is a dimensionless constant ($k = 0.4$, see Simiu and Scanlan 1996); z is altitude; z_0 is the ground roughness height; z_d is defined as

$$z_d = \bar{H} - z_0 / k \quad (10)$$

where \bar{H} is the mean height of the buildings around.

For description of the turbulence profile, we define two dimensionless coefficients related to the turbulence intensity, as

$$\beta_u = \sigma_u / u_* \quad (11)$$

$$\beta_w = \sigma_w / u_* \quad (12)$$

where σ_u and σ_w are respectively the RMS values of the along-wind and vertical turbulence components.

According to Eq. (9), the following turbulence profiles are targeted

$$I_u(z) = \frac{0.4\beta_u}{\ln[(z - z_d) / z_0]} \quad (13)$$

and

$$I_w(z) = \frac{0.4\beta_w}{\ln[(z - z_d) / z_0]} \quad (14)$$

According to field observations, Tieleman (2008) determined that $\beta_u = 2.5$ and $\beta_w = 0.5\beta_u$, which is also employed by the wind-resistant specification for highway bridge in China. Therefore, the following turbulence profiles are obtained accordingly

$$I_u(z) = \frac{1}{\ln[(z - z_d) / z_0]} \quad (15)$$

$$I_w(z) = 0.5I_u(z) \quad (16)$$

Dyrbye and Hansen (1997) suggested the following integral scales of turbulence in the along-wind direction

$$L_u^x = \begin{cases} 100(0.1z)^{0.3} & 10m \leq z \leq 200m \\ 100 & z \leq 10m \end{cases} \quad (17)$$

and

$$L_w^x = 0.4z \quad (18)$$

In the current section, the Kaimal, Panofsky, and von Kármán's wind spectra (Simiu and Scanlan 1996) are employed for different purposes, and different wind fields can be simulated by changing the values of I_u , I_w , L_u , and L_w .

The spectra of along-wind and vertical fluctuations, denoted in terms of the von Kármán spectra, are given as

$$S_u(n) = \frac{4(I_u(z)U(z))^2(L_u(z)/U(z))}{\left[1 + 70.8(nL_u(z)/U(z))^2\right]^{5/6}} \quad (19)$$

$$S_w(n) = \frac{4(I_w(z)U(z))^2(L_w(z)/U(z))(1 + 188.4(2n(L_w(z)/U(z))))^2}{\left[1 + 70.8(nL_u(z)/U(z))^2\right]^{11/6}} \quad (20)$$

The along-wind Kaimal spectrum is expressed as

$$S_u(n) = 200u_*^2 \frac{f}{n(1 + 50f)^{5/3}} \quad (21)$$

where $f = nz/U(z)$.

The Panofsky spectrum, used for vertical wind fluctuations, is given as follow

$$S_w(n) = 6u_*^2 \frac{f}{n(1 + 4f)^2} \quad (22)$$

Spacial coherence of the turbulence used in this study is defined as

$$\rho(r) = \frac{\int_0^{+\infty} S_{AB}(\bar{x}_1, \bar{x}_2, \omega) d\omega}{\sqrt{\int_0^{+\infty} S_A(\bar{x}_1, \omega) d\omega} \sqrt{\int_0^{+\infty} S_B(\bar{x}_2, \omega) d\omega}} \quad (23)$$

where $S_A(\bar{x}_1, \omega)$ and $S_B(\bar{x}_2, \omega)$ are respectively the PSDs corresponding to the two points \bar{x}_1 and \bar{x}_2 , and r is the spacial distance between these two points. When the Kaimal spectrum is used, for example, the spacial coherence coefficient is

$$\rho(r) = \frac{\int_0^{+\infty} \sqrt{\frac{1}{(1 + K_1)^{5/3}}} \sqrt{\frac{1}{(1 + K_2)^{5/3}}} e^{-\hat{f}} d\omega}{\sqrt{\int_0^{+\infty} \frac{1}{(1 + K_1)^{5/3}} d\omega} \sqrt{\int_0^{+\infty} \frac{1}{(1 + K_2)^{5/3}} d\omega}} \quad (24)$$

where $K_i = 50 \frac{\omega z_i}{2\pi U(z_i)}$ ($i=1, 2$).

The cross-PSD function between two point A and B used in this study is expressed by

$$S_{AB}(\bar{x}_1, \bar{x}_2, \omega) = \sqrt{S_A(\bar{x}_1, \omega)} \sqrt{S_B(\bar{x}_2, \omega)} e^{-\hat{f}} \quad (25)$$

where

$$f = \frac{\omega[C_z^2(z_1 - z_2)^2 + C_y^2(y_1 - y_2)^2 + C_x^2(x_1 - x_2)^2]^{1/2}}{\pi[U(z_1) + U(z_2)]} \quad (26)$$

where y_1, y_2, z_1, z_2 are respectively the vertical and lateral coordinates of the two points; $U(z_1), U(z_2)$ are the mean wind speeds corresponding respectively to the height z_1 and z_2 ; C_y, C_z are constants relating to spacial correlation properties.

Once the wind fields are simulated, wind load fluctuations developed on the bridge deck (per unit span) can be determined based on quasi-steady assumptions, as

$$D_b(x, t) = \frac{1}{2} \rho U^2 B \left(2C_D \frac{u(x, t)}{U} + C'_D \frac{w(x, t)}{U} \right) \quad (27)$$

$$L_b(x, t) = \frac{1}{2} \rho U^2 B \left(2C_L \frac{u(x, t)}{U} + (C'_L + C'_D) \frac{w(x, t)}{U} \right) \quad (28)$$

$$M_b(x, t) = \frac{1}{2} \rho U^2 B^2 \left(2C_M \frac{u(x, t)}{U} + C'_M \frac{w(x, t)}{U} \right) \quad (29)$$

where $D_b(x, t)$, $L_b(x, t)$ and $M_b(x, t)$ denote the buffeting drag, lift and pitching moment, respectively, x denotes the bridge axis direction, ρ is the air density. C_L, C_D, C_M are the aerostatic lift, drag and pitching moment force coefficients, respectively, which are functions of the effective wind angle of attack, as shown in Fig. 12; B is the reference width of the bridge deck; $u(x, t)$, $w(x, t)$ are the longitudinal and vertical wind fluctuations, respectively. It is noted that aerodynamic admittance in this paper is taken as constant 1.

Referring to Fig. 14, the instantaneous quasi-steady wind loads exerted on the main cables (per unit length) can be expressed as

$$D(\mathbf{x}, t) = \frac{1}{2} \rho C_D d \left\{ [U(\mathbf{x}) + u(\mathbf{x}, t)]^2 + \tilde{w}^2(\mathbf{x}, t) \right\} \quad (30)$$

where D is the drag in the instantaneous wind direction, \mathbf{x} the space vector, d the diameter of the main cable and $\tilde{w}(\mathbf{x}, t)$ the component of $w(\mathbf{x}, t)$ perpendicular to the cable elements.

With expression (30), the fluctuating component in the mean wind direction can be readily obtained as

$$D_b(\mathbf{x}, t) = \frac{1}{2} \rho C_D d \left\{ [U(\mathbf{x}) + u(\mathbf{x}, t)]^2 + \tilde{w}^2(\mathbf{x}, t) \right\} \cos \alpha - \frac{1}{2} \rho C_D d U^2(\mathbf{x}) \quad (31)$$

and the fluctuating component perpendicular to both the mean wind direction and the cable axis is

$$\tilde{L}_b(\mathbf{x}, t) = \frac{1}{2} \rho C_D d \left\{ [U(\mathbf{x}) + u(\mathbf{x}, t)]^2 + \tilde{w}^2(\mathbf{x}, t) \right\} \sin \alpha \quad (32)$$

where in formulae (31) and (32), α is determined by

$$\alpha(\mathbf{x}, t) = \arctan \frac{\tilde{w}(\mathbf{x}, t)}{U(\mathbf{x}) + u(\mathbf{x}, t)} \quad (33)$$

4.3 Sensitivity to wind spectra

Time-domain buffeting analyses of the bridge have been performed with two different wind fields taken into account. The Kaimal and von Kármán's spectra are used for the simulation of the longitudinal wind fields, and the Panofsky's and von Kármán's spectra are used to simulate the vertical wind fields. Comparisons among these wind spectra are plotted in Fig. 15, where distinctions can be seen in both the distribution of wind energy and the predominant frequency.

Fig. 16 plots the results when Kaimal and Panofsky spectra are used respectively for simulations of longitudinal and vertical turbulence. Hangers most susceptible to BIR are S2 and M2 (the second ones from the tower to the side-span and mid-span, respectively). This is in accordance with findings reported by Zhang *et al.* (2015), although the FE model in the present work is updated and the dominant frequency of BIR decreases slightly.

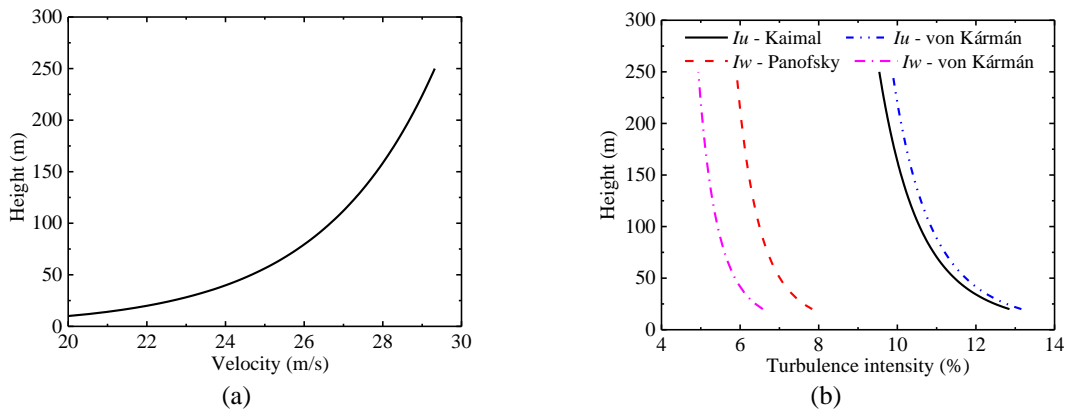


Fig. 13 Wind profiles: (a) Mean wind and (b) turbulence intensity

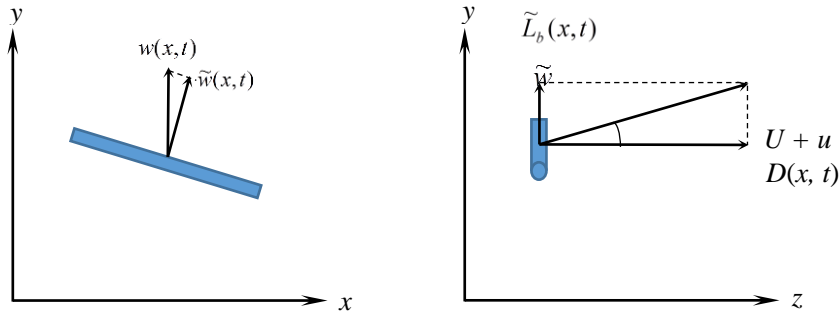


Fig. 14 Direction of wind fluctuations acting on the main cable

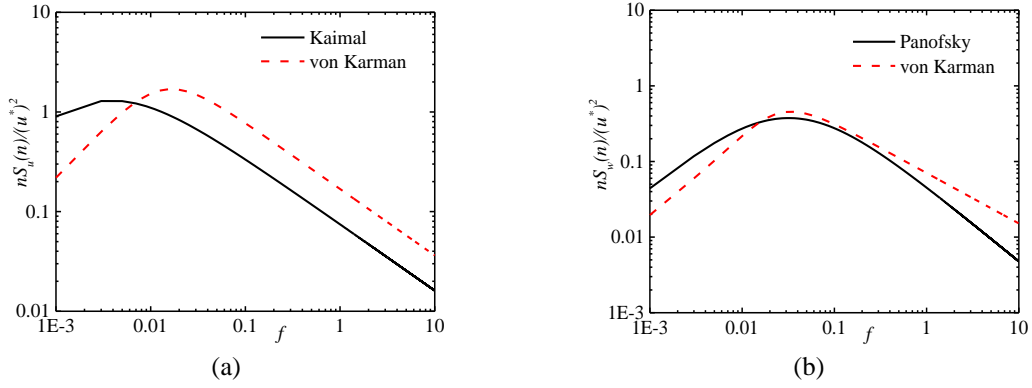
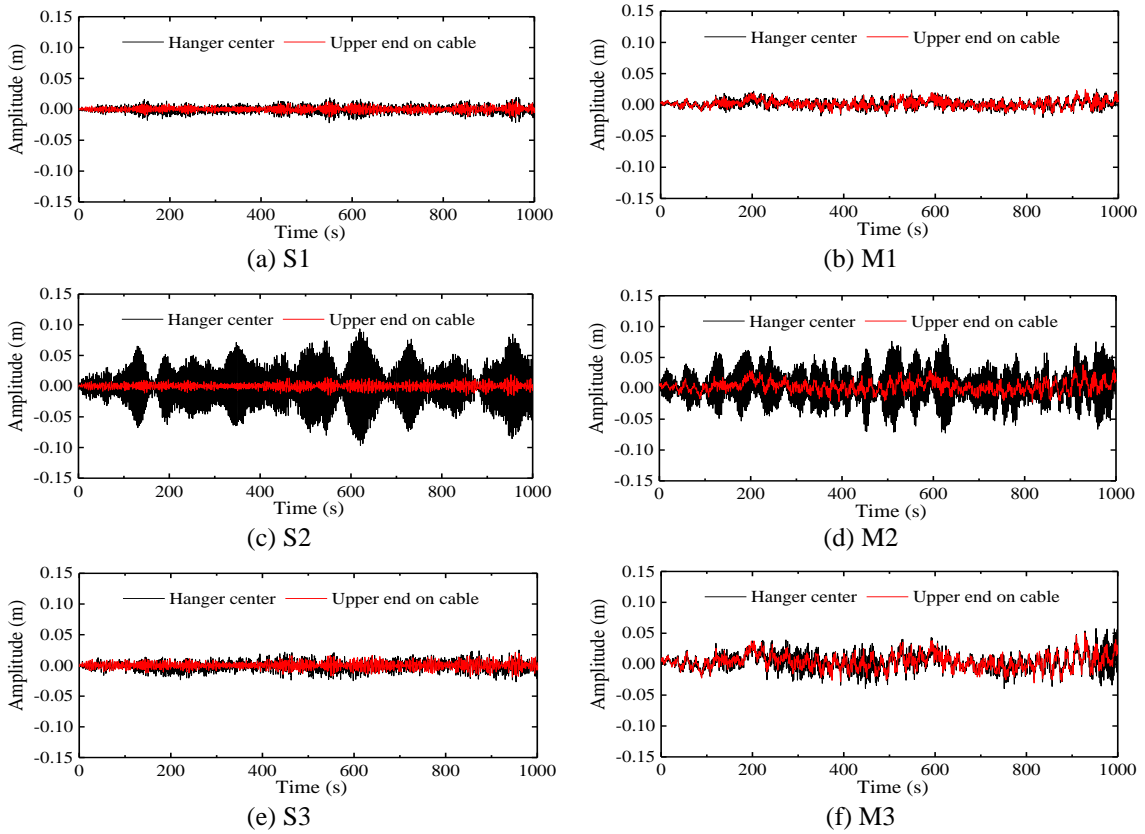


Fig. 15 Power spectra of wind fluctuations: (a) Longitudinal and (b) Vertical



Continued-

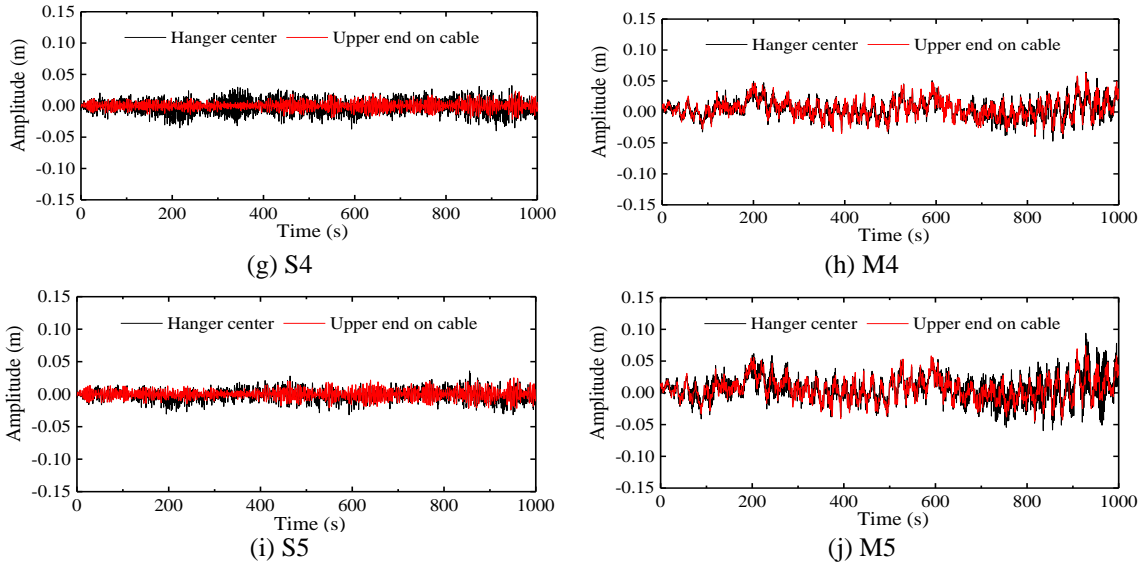


Fig. 16 Lateral responses of hangers resulted from Kaimal and Panofsky wind spectra

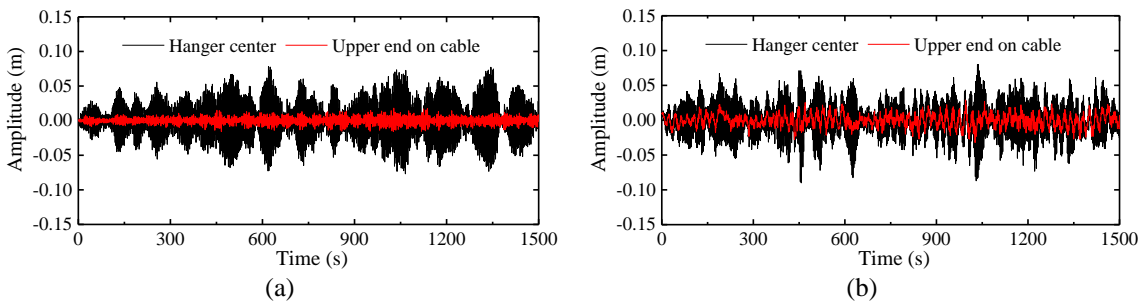


Fig. 17 Lateral responses of hangers resulted from von Kármán wind spectra: (a) hanger S2 and (b) hanger M2

It is noted the response of an upper end represents the response of the main cable at the position where a hanger is attached. Hangers from S1 to S5 (or M1 to M5, see Fig. 10) are progressively away from the bridge tower where the main cable is fixed; therefore, buffeting responses at upper ends of S1 to S5 are also becoming progressively intense. However, obvious BIR occurs only to S2 and M2, which are the second closest ones to the tower, and hence should have the second smallest excitations.

Fig. 17 plots the main results when von Kármán's spectrum is used. Similar to those shown in Fig. 16, hangers S2 and M2 exhibit obvious resonant oscillation while others not. Hence, for the sake of concision, only responses of hangers S2 and M2 are presented. By comparing Fig. 17(a) with Figs. 16(c), and 17(b) with Fig. 16(d), it is noticed that no significant difference in BIR exists between the results from the two wind fields. Hence, as far as these two cases are concerned, the BIR of the hangers on this bridge is insensitive to the type of wind spectrum selected.

4.4 Sensitivity to turbulence intensity

Based on the von Kármán wind spectrum, wind fields of different turbulence intensities are simulated, of which the main properties are listed in Table 1. While the turbulence intensities change, their spacial correlations of wind fluctuations keep unchanged. Based on these three wind fields, time-domain buffeting simulations of the whole structure have been conducted. The main results are presented; Figs. 18 and 19 plot respectively time histories and amplitude spectra of S2, and Figs. 20 and 21 plot respectively time histories and amplitude spectra of M2. It is noticed that with turbulence intensity increases progressively from I_u at wind field 1 to $1.8I_u$ at wind field 3, the responses of both hangers S2 and M2 increase obviously, approximately proportional to the turbulence intensity. It is also noticed from the spectra that the amplitude culminates at about 0.4 Hz, which corresponding to the dominant oscillating frequency of the hangers.

Table 1 Wind field properties

| Wind field | Turbulence intensity | | Integral length scale | |
|------------|----------------------|-----------|-----------------------|----------|
| | Horizontal | Vertical | Horizontal | Vertical |
| field 1 | I_u | I_w | L_u | L_w |
| field 2 | $1.4*I_u$ | $1.4*I_w$ | L_u | L_w |
| field 3 | $1.8*I_u$ | $1.8*I_w$ | $0.6*L_u$ | L_w |

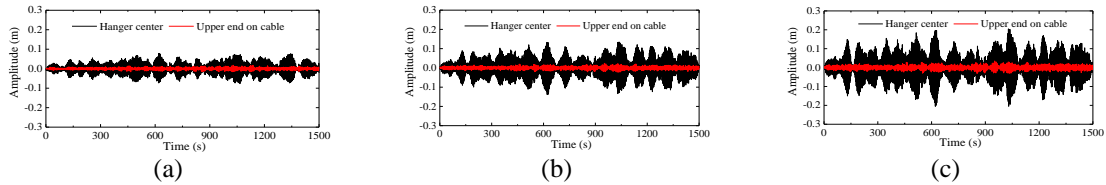


Fig. 18 Time histories of hanger S2: (a) in wind field 1, (b) in wind field 2 and (c) in wind field 3

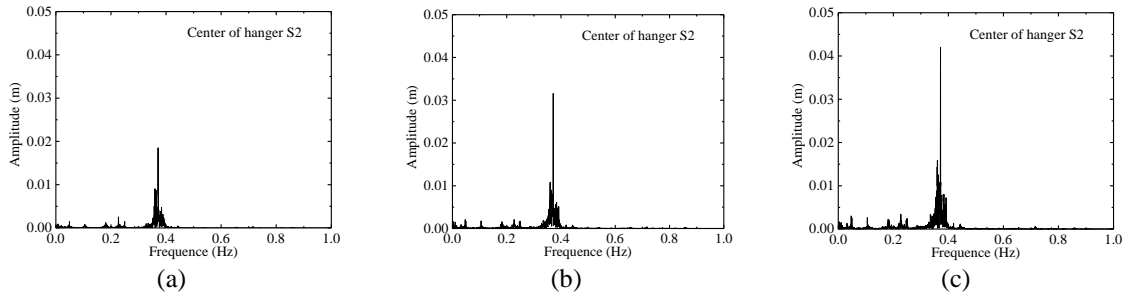


Fig. 19 Amplitude spectra of S2: (a) in wind field 1, (b) in wind field 2 and (c) in wind field 3

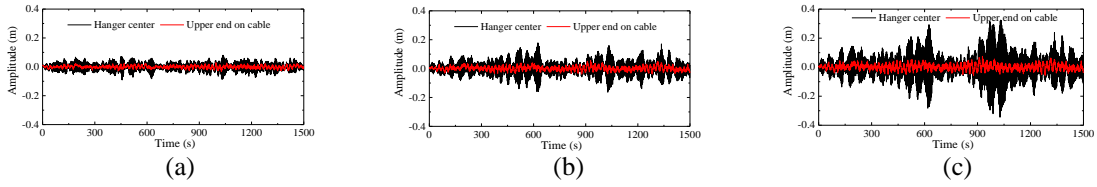


Fig. 20 Time histories of hanger M2: (a) in wind field 1, (b) in wind field 2 and (c) in wind field 3

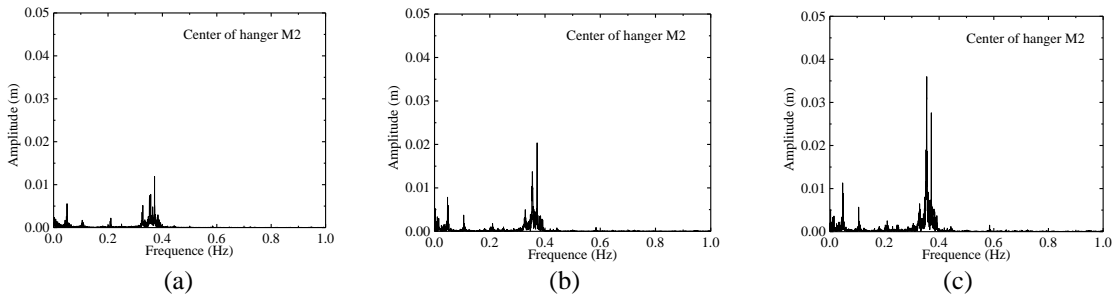


Fig. 21 Amplitude spectra of M2: (a) in wind field 1, (b) in wind field 2, (c) in wind field 3

Referring to Fig. 22, it is favorable to define a resonance factor β as

$$\beta = \frac{d_h}{d_c} \tag{26}$$

where d_c is the amplitude of the main cable at the position where the concerned hanger is attached, and d_h is the vibrating amplitude at the center of the hanger.

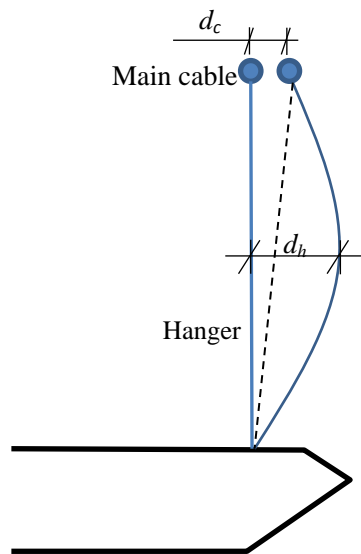
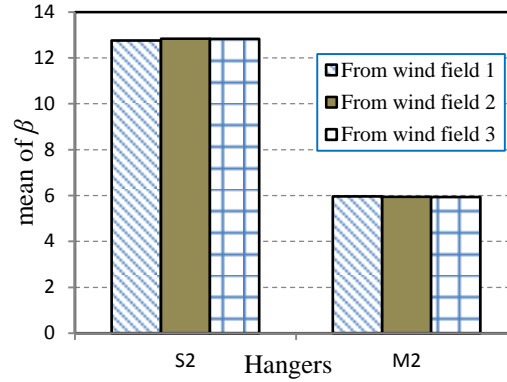


Fig. 22 Figure used for definition of β

Fig. 23 Mean values of β

It is shown that the BIR of the hangers is not stable, exhibiting intermittency in time domain. Therefore, the resonance factors should also be time-varying. However, the intensity of BIR could be reflected by the mean values of the resonance factor β over time, which are plotted in Fig. 23. It is noticed that, obviously, no perceptible differences are found among the three cases; that is, resonance factor β keep unchanged even when the amplitudes of BIR increase or decrease drastically. Hence, it is not the BIR itself being sensitive to the turbulence intensity, but instead, the buffeting responses of the main cables.

4.5 Sensitivity to spacial coherence of turbulence

Based on Kaimal's (for along-wind fluctuation) and Panofsky's (for vertical fluctuation) spectra, three wind fields differ in spacial coherence are simulated, aiming to investigate their effects on the BIR. Referring to Eq. (26), the spacial coherence is actually determined by the three coefficients C_x , C_y , and C_z . In the atmospheric boundary layer, all these coefficients change with the mean wind speed and the altitude. Based on what have observed, they can vary in a quite wide range from 3 to 50 (Shiotani and Iwatani 1972, Kristensen and Jensen 1979, Kristensen *et al.* 1981, Simiu and Scanlan 1996). Different spacial coherences are realized via adjustment of the constants C_x , C_y and C_z , listed in Table 2. The spacial correlation coefficients, targeted and simulated, are plotted in Fig. 24.

Table 2 C_x , C_y and C_z used for wind fields simulation

| | Case 1 | Case 2 | Case 3 |
|-------|--------|--------|--------|
| C_x | 3 | 3 | 3 |
| C_y | 8 | 16 | 30 |
| C_z | 7 | 10 | 20 |

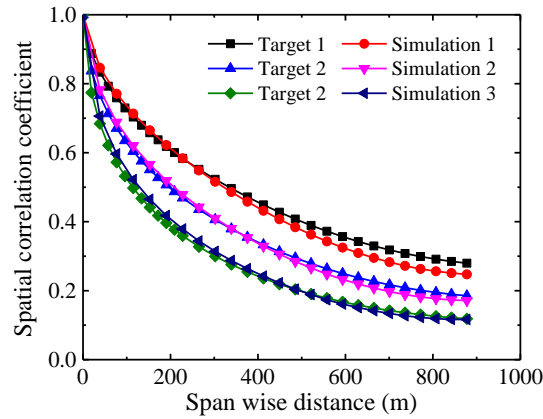


Fig. 24 Spatial correlation coefficients

Responses of hangers S2 and M2 are plotted in Fig. 25, and corresponding amplitude spectra are plotted in Fig. 26. Both figures indicate that the BIR of the two hangers, S2 and M2, is insensitive to the concerned range of spacial coherences. Since the BIR of the hangers is induced by the buffeting of the main cable, at a specific vibrating frequency, this insensitivity reflects indirectly that the buffeting of the main cables at this frequency is weakly affected by the spacial coherence of wind fluctuations ranged as listed in Table 2. However, it should be realized that this by no means indicate spacial coherence of wind fluctuations has little effects on the buffeting of the main structure, as listed in Table 3 in terms of RMS values of the bridge deck and main cable. Obviously, the spacial coherence affects substantially the buffeting responses of the bridge deck, and the main cables at quarter and mid-span. The buffeting of the main cable at the position where S2 attached, however, is little affected by the wind fields, showing the buffeting at this position is dominated by high-order modes which are insusceptible to the wind correlation as ranged.

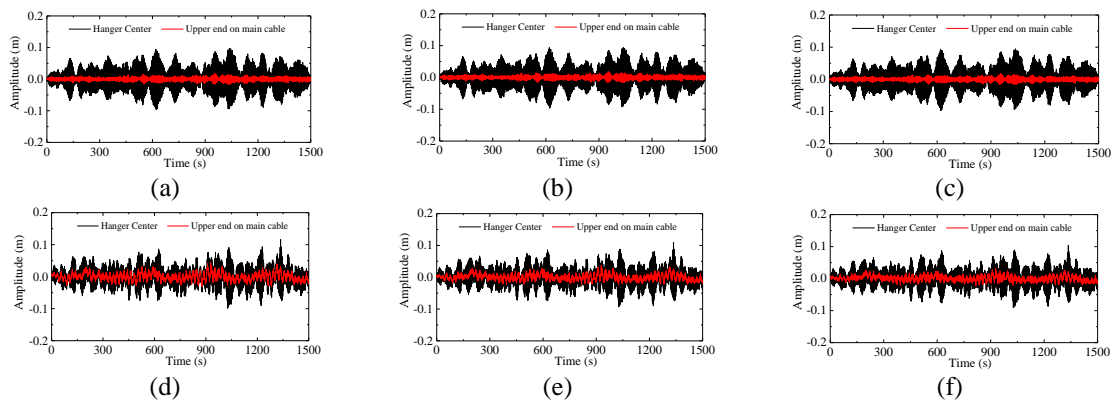


Fig. 25 Time histories of hangers under various wind fields: (a) S2 in wind field 1, (b) S2 in wind field 2, (c) S2 in wind field 3, (d) M2 in wind field 1, (e) M2 in wind field 2 and (f) M2 in wind field 3

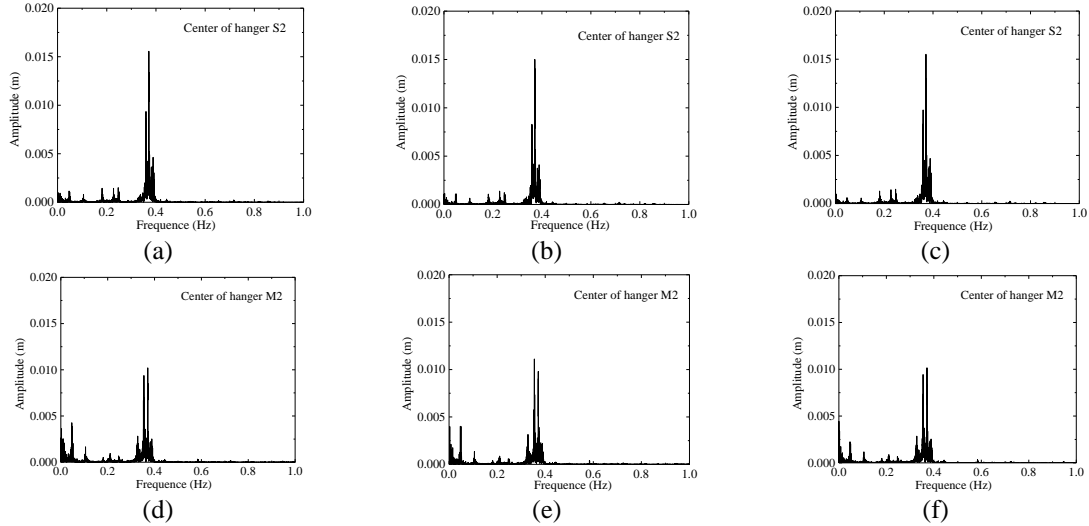


Fig. 26 Amplitude spectra of hangers: (a) S2 in wind field 1, (b) S2 in wind field 2, (c) S2 in wind field 3, (d) M2 in wind field 1, (e) M2 in wind field 2 and (f) M2 in wind field 3

Table 3 RMS values of the main structure

| Wind field | RMS of bridge deck (mid-span) | | | Lateral RMS of the main cable (m) | | | |
|------------|-------------------------------|--------------|-----------------|-----------------------------------|----------|--------|--------|
| | Lateral (m) | Vertical (m) | Torsional (rad) | 1/4 span | mid-span | at S2 | at M2 |
| field 1 | 0.158 | 0.275 | 0.0027 | 0.104 | 0.146 | 0.0044 | 0.0113 |
| field 2 | 0.125 | 0.277 | 0.0026 | 0.082 | 0.115 | 0.0043 | 0.0093 |
| field 3 | 0.105 | 0.278 | 0.0026 | 0.068 | 0.097 | 0.0043 | 0.0083 |

4.6 Vibration reduction

Since the frequency-matching of the cable and hangers is vital to the BIR, it is favorable to change the natural frequencies of those hangers susceptible to BIR. The dynamic properties of a hanger at suspension bridges is exactly like those of a pre-tensed flexible cable, natural frequencies of which are determined by length, tension, and linear mass density. The length and tension of a hanger are determined respectively by the structural configuration and the dead load properties of the bridge deck, and hence little space is left for adjustments. The linear mass density, however, is able to be altered substantially if we replace the steel rope with carbon fiber reinforced polymer (CFRP). For comparison, main properties of the steel strand and CFRP are listed in Table 4. It is noticed that the linear mass density of CFRP is as small as just one fifth of that of the steel strand. Therefore, the natural frequencies of a CFRP hanger could increase approximately 2.3 times of those otherwise similar steel hanger.

Table 4 Material properties of CFRP and steel strand

| Property | CFRP | Steel strand |
|----------------------------|------|--------------|
| Tensile strength (MPa) | 2800 | 1860 |
| Modulus of elasticity(GPa) | 160 | 195 |
| Density (t/m^3) | 1.5 | 7.85 |
| Elongation (%) | 1.6 | 7.0 |

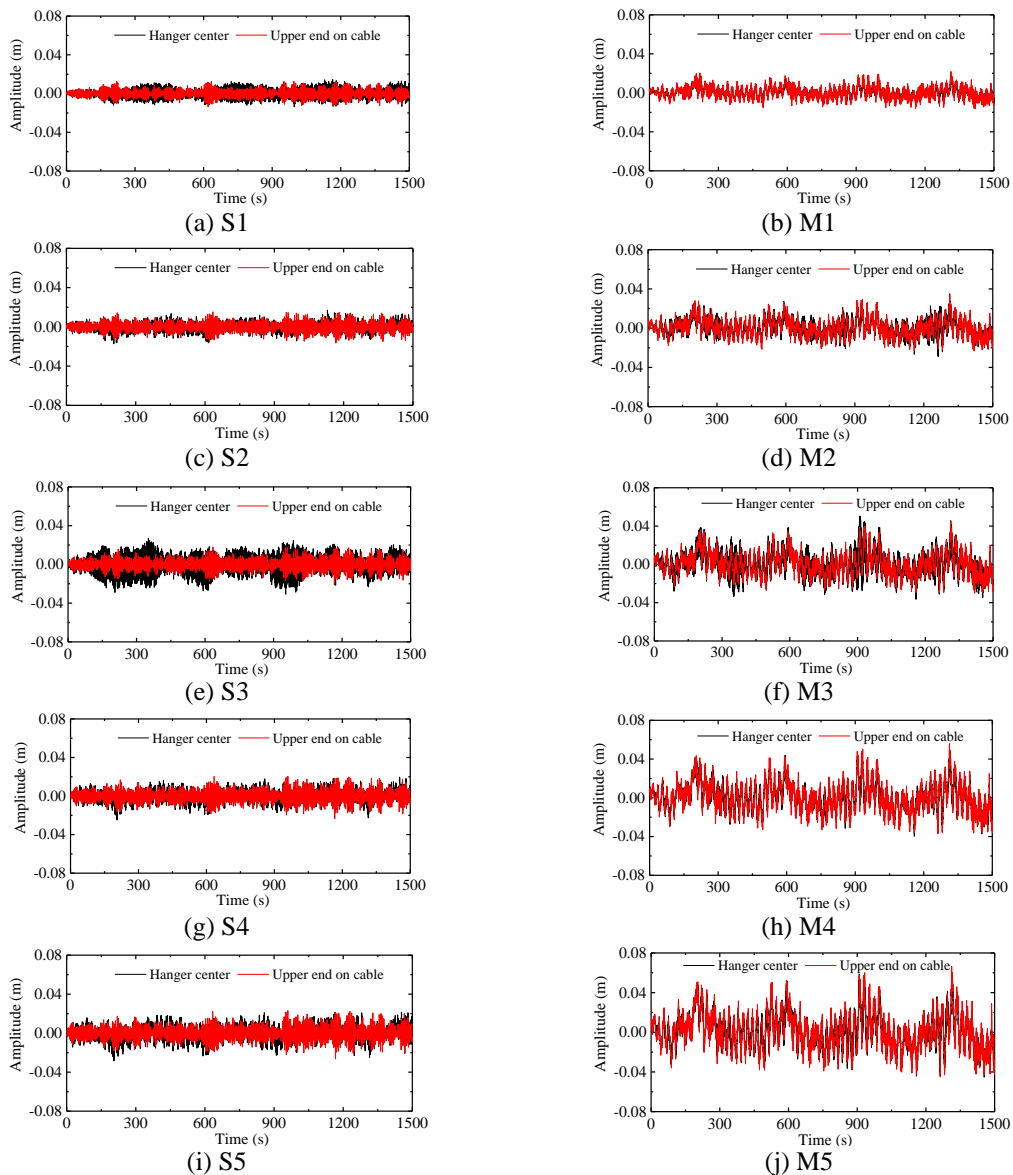


Fig. 27 Displacement time histories of the hangers and the supporting points on the main cables (CFRP)

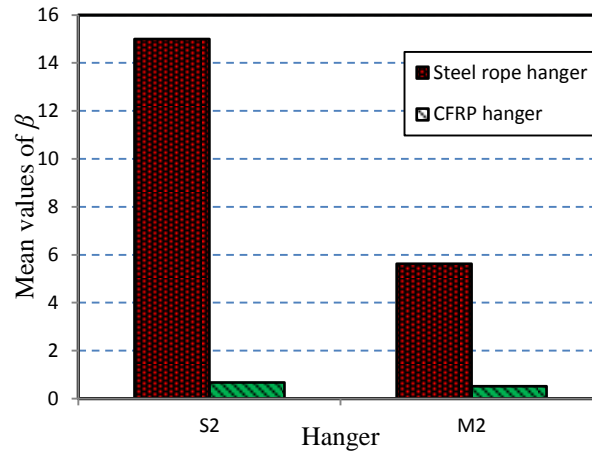


Fig. 28 Resonance factors of S2 and M2

The CFRP hangers in the FE model are designed so that the safety factors are the same as those of the original steel ropes. The resulting effects are significant, as can be seen from the time histories plotted in Fig. 27. The BIR of the hangers S2 and M2, obvious for all cases with steel ropes, disappears now with the CFRP hangers. The extent of vibration reduction is also been indicated from the drop of resonance factors, as plotted in Fig. 28, against the original ones with steel hangers. Resonance factors of both S2 and M2 drop drastically from 15.0 and 5.6 to 0.66 and 0.51, respectively, showing a substantial reduction in BIR.

5. Conclusions

In virtue of a numerical example, this paper addresses the BIR of hangers on long-span suspension bridges, phenomena of which has been reported for many years yet mechanism has not been fully understood. The following conclusions are drawn based on discussions presented: (i) The BIR of hangers on long-span suspension bridges are induced by the buffeting responses of the main cables; (ii) As far as the range of investigation presented, no significant difference in the BIR has been found between the two types of wind spectrum concerned; (iii) The turbulence intensity of the wind field dominates the buffeting responses of the main cables, and as a result, affects the amplitude of BIR of the hangers. However, its effects on the resonance factor, the ratio of the response of hanger to that of the main cable, are negligibly small; (iv) The spacial coherence of the wind fluctuations, within the range considered, show little effects on the BIR of the hangers, even though it changes obviously the buffeting of the main structure; (v) Replacement of steel hangers with CFRP material can be a very effective countermeasure against BIR, by increasing substantially the natural frequencies of the hangers.

Acknowledgements

Authors are grateful to the financial support from the National Science Foundation of China

(Grant Number 51578233, 51178182) to the work described in this paper. Authors also wish to thank the reviewers for their dedicated suggestions and comments to this work.

References

- Cheng, S., Tanaka, H., Larose, G.L. and Savage, M.G. (2003), "Aerodynamic behavior of an inclined circular cylinder", *Wind Struct.*, **6**(3), 197-208.
- Cigada, A., Diana, G., Falco, M., Fossati, F. and Manenti A. (1997), "Vortex shedding and wake-induced vibrations in single and bundle cables", *J. Wind Eng. Ind. Aerod.*, **72**(1), 253-263.
- Deodatis, G. (1996), "Simulation of ergodic multivariate stochastic processes", *J. Eng. Mech. - ASCE*, **122**(8), 778-787.
- Dyrbye, C. and Hansen, S.O. (1997), *Wind Loads on Structures*, John Wiley & Sons Ltd., Chichester, England, UK.
- Hikami, Y. and Shiraishi, N. (1988), "Rain-wind induced vibrations of cables stayed bridges", *J. Wind Eng. Ind. Aerod.*, **29**(1-3), 409-418.
- Kristensen, L. and Jensen, N. O. (1979), "Lateral coherence in isotropic turbulence and in the natural wind", *Bound. -Lay. Meteorol.*, **17**(3), 353-373.
- Kristensen, L., Panofsky, H.A. and Smith, S.D. (1981), "Lateral coherence of longitudinal wind components in strong winds", *Bound. -Lay. Meteorol.*, **21**(2), 199-205.
- Laursen, E., Bitsch, N. and Andersen, J.E. (2006). "Analysis and mitigation of large amplitude cable vibration at the Great Belt East bridge", *Proceedings of the IABSE Conference*, Copenhagen, July.
- Macdonald, J.H.G. and Larose, G.L. (2006), "A unified approach to aerodynamic damping and drag/lift instabilities, and its application to dry inclined cable galloping", *J. Fluids Struct.*, **22**(2), 229-252.
- Matsumoto, M., Shirato, H., Yagi, T., Goto, M., Sakai, S. and Ohya, J. (2003), "Field observation of the full-scale wind-induced cable vibration", *J. Wind Eng. Ind. Aerod.*, **91**(1-2), 13-26.
- Matsumoto, M., Yagi, T., Hatsuda, H., shima, T., Tanaka, M. and Naito H. (2010). "Dry galloping characteristics and its mechanism of inclined/yawed cables", *J. Wind Eng. Ind. Aerod.*, **98**(6-7), 317-327.
- Miyata, T., Yamada, H. and Hojo, T. (1994), "Aerodynamic response of PE stay cables with pattern-indented surface", *Proceedings of the International Conference on Cable-Stayed and Suspension Bridges (AFPC)*, Deauville, March.
- Price, S.J. (1975), "Wake induced flutter of power transmission conductors", *J. Sound Vib.*, **38**(1), 125-147.
- Raeesi, A., Cheng, S. and Ting, D.S. (2013), "Aerodynamic damping of an inclined circular cylinder in unsteady flow and its application to the prediction of dry inclined cable galloping", *J. Wind Eng. Ind. Aerod.*, **113**(1), 12-28.
- Shiotani, M. and Iwatani, Y. (1972), "Correlations of wind velocities in relation to the gust loadings", *Proceedings of the 3rd International conference on wind effects on buildings and structures*, Tokyo, May.
- Simiu, E. and Scanlan, R.H. (1996), *Wind Effects on Structures Fundamentals and Applications to Design*, John Wiley & Sons, Inc., New York., NY, USA.
- Tieleman, H.W. (2008), "Strong wind observations in the atmospheric surface layer", *J. Wind Eng. Ind. Aerod.*, **96**(1), 41-77.
- Zhang, Z.T. and Ge, Y.J. (2015), "Buffeting induced resonance of hangers on a suspension bridge", *Proceedings of the 14th ICWE*, Porto Algre, June.
- Zhang, Z.T., Wu, X.B., Chen, Z.Q. and Ge, Y.J. (2016), "Mechanism of a kind of hanger oscillation at suspension bridges: Buffeting induced resonance", *J. Bridge Eng.- ASCE*, **21**(3).
- Zuo, D. and Jones, N. P. (2010). "Interpretations of field observations of wind- and rain-wind-induced stay cable vibrations", *J. Wind Eng. Ind. Aerod.*, **98**(2), 73-87.